

Stimulated Emission from Rhodamine 6G Aggregates Self-Assembled on Amyloid Protein Fibrils

Piotr Hanczyc,[†] Lech Sznitko,[‡] Chengmei Zhong,[†] and Alan J. Heeger^{*,†}

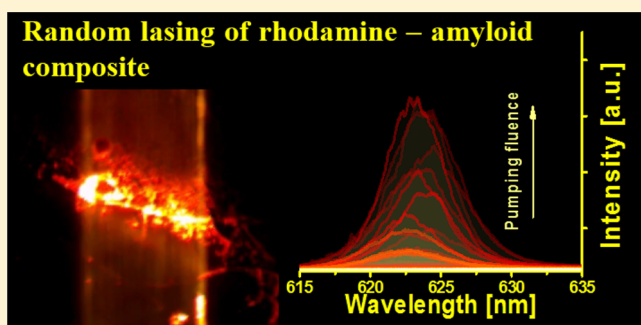
[†]Center for Oligomers & Organic Solids, University of California, Santa Barbara, 2520A Physical Sciences Building North, Santa Barbara, United States

[‡]Advanced Materials Engineering and Modelling Group, Faculty of Chemistry, Wrocław University of Technology, 50-370, Wrocław, Poland

Supporting Information

ABSTRACT: Amyloid fibrils are excellent bioderived nanotemplates for controlling molecular and optical properties of small molecules such as organic dyes. Here we demonstrate that two representative fibril-forming proteins, lysozyme and insulin, from the amyloids family can determine the optical signature of rhodamine 6G. Their structural variety leads to a unique molecular arrangement of dye aggregates on the biotemplate surface. This significantly influences the light amplification threshold as well as the stimulated emission profiles, which show remarkable broadband wavelength tunability. We show in addition that amyloid fibrils can be potentially used in constructing broadband emission biolasers.

KEYWORDS: amyloid fibrils, lysozyme and insulin proteins, stimulated emission, random lasing, laser dye, rhodamine 6G, biolaser, biomaterial, nanotemplates, molecular crowding



Amyloid fibrils are a hallmark of neurodegenerative diseases.^{1,2} Since their discovery, research has focused on understanding their formation, progression, and structural features.³ Molecular studies indicate that amyloid fibrils are unique biopolymers with rich diversity where β -sheet structures are predominant.⁴ The studies revealed also their interesting material properties, where rigidity of a single fibril of different protein source can range from highly flexible (90–320 MPa)⁵ to extremely stiff (2–14 GPa).⁶ The diversity and self-assembling properties of amyloid fibrils make them attractive nanomaterials for supramolecular complexation of small molecules.

In this article we expand our previous research on amyloid–dye complexes⁷ to two types of amyloid-forming proteins, insulin and lysozyme, that were doped with rhodamine 6G. Organic fluorophores are well known for high affinity to amyloid fibrils.^{8–11} However, the rhodamine family of dyes is particularly interesting because of both medical and technological relevance. Its derivatives have been used as staining agents, for example, monitoring the drug uptake at the blood–brain barrier in Alzheimer’s therapy.¹² On the other hand they are suitable and often fluorophores of choice for laser construction because of convenient photophysical features.¹³

Here we show that rhodamine 6G-stimulated emission profiles are related to the intrinsic structure of the amyloid protein fibrils and their material properties. Rhodamine 6G interacting with fibrils enables extending classical spectroscopic characterization of amyloid–dye complexation using laser

spectroscopy, as was presented previously for DNA^{14–16} and silk fibroins.^{17,18} Our experiments indicate that the biophotonics that was previously related only to DNA and DNA complexes can be expanded to a broader spectrum of biologically derived materials such as amyloid-forming proteins. We show not only that processes between biomolecules and chromophores (e.g., intercalation, groove binding) may be utilized to tailor photonic properties of biomaterials but also that molecular crowding and interactions with second-order structures of these materials are relevant to the optical signatures. Proteins are particularly interesting due to their ability to generate higher order species through self-assembly. Moreover, there are many possible interactions with different dyes as a result of electrostatic and/or van der Waals interactions. These different supramolecular complexes may become crucial for designing future biobased materials for photonics. Moreover they are biofriendly, the production does not require oil or other nonrenewable sources, and often they can have a diagnostic capability.

Here we show that stimulated emission spectra and random lasing provide information about chromophore–chromophore interactions within the binding sites in the supramolecular complexes. Fluorophore stimulated emission (SE) spectra significantly vary depending on the protein source. Therefore, the SE spectra provide indirect information about the intrinsic

Received: August 13, 2015

structure of amyloid fibrils. Since these two types of amyloid-forming proteins resemble the structure of the vast majority of disease-related pathogenic specimens, stimulated emission and random lasing might provide additional information in biosample analysis, e.g., recognition of various amyloids in cerebrospinal fluids (CSF).

The structural polymorphism of amyloid fibrils affects the thin-film morphology and thereby the mechanism of light amplification. Molecular crowding enhances the optical signals and shows the potential of amyloid fibrils in technological applications, e.g., bioderived lasers where biotemplates' intrinsic properties can determine the function of biodevices.

The key finding of our work is the demonstration that the type of amyloid fibrils determines the size and shape of rhodamine 6G aggregates at bioderived nanotemplate surfaces, as monitored by recording the fluorophore-stimulated emission spectra.

MATERIALS AND METHODS

Experimental Section. Native monomers of lysozyme protein from chicken egg white and insulin protein from bovine pancreas were purchased from Sigma-Aldrich, dissolved to 10 mg/mL in pH = 2 (0.01 M HCl) water, and used as the stock solution concentration. The solutions were filtered through a 0.2 μm filter and heated to 65 $^{\circ}\text{C}$ for 6 days and 24 h, respectively. After fibril formation the samples were centrifuged at 3000 rpm for 3 min in order to remove globular particulates. The stock solution of rhodamine 6G dye was prepared by dissolving 5 mg/mL of the laser dye in water. For all solution experiments the stocks of Rh6G and amyloids were diluted to 0.05 and 0.1 mg/mL, respectively. For thin-film preparation, dye and amyloid fibril stock solutions were mixed in 1:20 of dye to biotemplate volume ratio and left for 1 h. The solid-state samples were prepared by casting on silica and left for drying for 24 h in ambient conditions.

UV–vis absorption spectra of amyloids–rhodamine complexes were recorded on a CARY-5000 spectrophotometer.

Linear dichroism is defined as the difference in absorbance of light linearly polarized parallel (A_{\parallel}) and perpendicular (A_{\perp}) to the macroscopic axis of orientation:

$$LD = A_{\parallel} - A_{\perp} \quad (1)$$

The LD spectra of amyloid fibrils doped with rhodamine 6G were recorded using a Chirascan CD spectrophotometer equipped with a quartz Couette cell for aligning the solute samples. In order to calculate the angle between the biopolymer macroscopic axis and the bound chromophore, the reduced LD (LD^r) is necessary. LD^r is a product of an orientation factor $0 < S < 1$ and optical factor O , which is the LD divided by the absorbance of the corresponding sample (A_{iso}),

$$LD^r = SO = \frac{LD}{A_{\text{iso}}} = \frac{3}{2}S(3\cos^2\alpha - 1) \quad (2)$$

In the case of amyloid fibril–chromophore interactions, the optical factor O is related to the angle α between the fibril axis and the light-absorbing transition moment of the dye. The orientation factor $S = 1/2(3\langle\cos^2\theta\rangle - 1)$ corresponds to the average orientation of the fibrils in a flow, where θ is the angle between the macroscopic orientation direction and the local amyloid fibril axis of a particular molecule and where the average runs over all amyloid fibrils in the sample. The binding angle α_{dye} of a specific transition dipole moment in a dye with

respect to the amyloid fibril axis can then be calculated from the LD^r value in its corresponding absorption band. In order to determine the binding angle α_{dye} , both LD^r and macroscopic orientation (S) must be known.

Transient absorption measurements were conducted with a femtosecond pulsed laser system at a repetition rate of 1 kHz as described previously in the literature.¹⁹ The laser used consists of a titanium sapphire oscillator (Spectra Physics Tsunami) that is pumped with a Nd:VO₄ laser (Spectra Physics Millennia). The pulses are fed into a regenerative amplifier (Spectra Physics Spitfire) that is pumped with a high-power Nd:YLF laser (Spectra Physics Empower); 790 nm pulses were generated with a pulse width of around 150 fs. The pulses were split into pump and probe paths. The pump pulse was frequency-doubled to 395 nm and focused onto the sample with a beam diameter of 1 mm and pulse energies of 30 $\mu\text{J}/\text{cm}^2$. The pump pulse was put through a digital delay stage to control pump–probe time delay. The probe pulse was focused into a 1 mm sapphire disk in order to generate the white light continuum used to measure the visible and near-IR spectra. The probe pulse was split before reaching the sample to provide a reference path to aid in the correction of intensity fluctuations. The subtraction was aided by careful collimation of the white light probe. In addition, synchronous chopping of the probe enabled the subtraction of an accurate dark count reading. All spectra were manually corrected for the temporal chirp present in the white light continuum. The polarization angle between pump and probe beams was 54 $^{\circ}$ (magic angle). Spectral data were collected with a silicon CCD camera that was calibrated using a series of narrow band-pass filters.

Fluorescence spectra were recorded using a Varian Cary Eclipse spectrofluorometer. The samples were excited at $\lambda_{\text{ex}} = 525$ nm and emission was recorded at $\lambda_{\text{em}} = 540$ –700 nm.

Stimulated emission in solution and solid samples was excited using the second harmonic ($\lambda = 532$ nm) from a Continuum Surelite II, Nd:YAG nanosecond pulsed laser. The excitation beam passed through a beam separator in order to spatially separate the third harmonic and the fundamental laser line. The excitation beam was then passed through a series of lenses providing beam shaping to achieve a uniform thin stripe of illuminated area in the sample plane. For thin films, the incoming light was incident normal to the sample surface. The edge emission from amyloid thin layers was collected using an Andor Shamrock 163 fiber spectrometer of spectral resolution around $\Delta\lambda \approx 0.1$ nm. In order to remove the scattered excitation light, a low-pass color filter was used at the entrance of the fiber.

Additionally a CCD camera equipped with an objective with magnification 5 \times was placed right after the biopolymer layers in order to check their magnified images in luminescent mode. A low-pass filter was used to filter out the excitation beam to prevent damaging the CCD camera. The experimental setup is presented in Figure S3 of the Supporting Information.

Thin film sample analysis was made using the LEXT OLS4000 3D laser measuring microscope that is designed for nanometer level imaging, 3D measurement, and roughness measurement.

RESULTS

Absorption and Linear Dichroism of Amyloid Fibrils Doped with Rhodamine 6G. The interactions of rhodamine 6G with lysozyme and insulin fibrils were examined in solution using UV–vis spectroscopy. Absorption spectra recorded for

pristine dye and in the presence of amyloids show nearly identical spectral features with the maximum at 525 nm (Figure 1) providing limited information about amyloid–chromophore

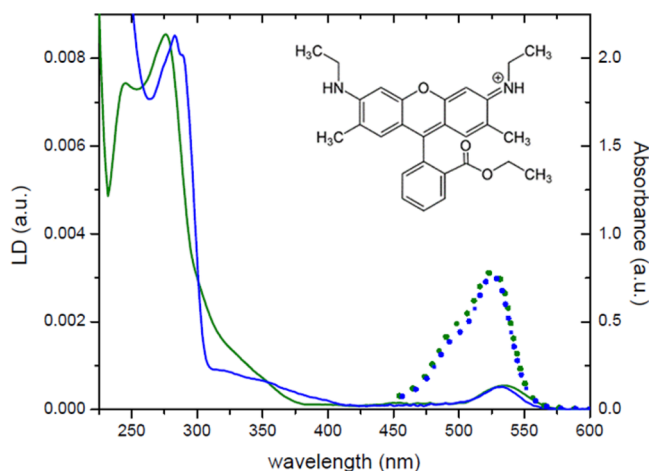


Figure 1. Absorbance (dotted) and linear dichroism of insulin fibrils (green solid) and lysozyme fibrils (blue solid) with rhodamine 6G (b).

interactions. Since rhodamine 6G molecules are positively charged and amyloid fibrils are highly protonated in acidic water (pH = 2), the linear dichroism technique was used in order to investigate whether the binding attraction is possible at all even if strong repulsive forces are dominant. Using the advantage of the LD that only the signal from flow oriented samples can be recorded, it is relatively easy to explore binding of small molecules to amyloids since free chromophores remain isotropic and give no contribution to the LD signal.

Recorded LD spectra (Figure 1) clearly show positive signals in the dye absorption band at 533 and 535 nm in the presence of lysozyme and insulin fibrils, respectively, indicating that rhodamine 6G molecules are attached at the amyloid surface. The small value of the calculated LD^* ($\sim 2 \times 10^{-4}$) at the dye absorption band prevents estimating the binding angle since α is close to the magic angle (54.7°), which is often the case for weak LD signals. There are two possible reasons of relatively weak chromophore orientation with respect to fibrils axis. One is that the benzene ring in rhodamine 6G substituted at xanthere is exposed to flow dynamics that can induce side-

chain motions and bending of the chromophore within the binding site at the amyloid surface. However, more plausible is that only a small fraction of dye molecules can bind to amyloid fibrils due to limited binding sites for positively charged dye molecules because of the highly protonated environment in pH = 2 solution. This hypothesis was partially confirmed by increasing the dye concentration in the amyloid-containing solution with no effect on the macroscopic alignment of the chromophore, indicating that only a small fraction of rhodamine molecules can bind to fibrils (results not shown), whereas the excess remains unbound. Together with the observation of a small red-shift (5 to 8 nm) in the LD spectrum when compared with the absorption of rhodamine monomers (525 nm), one can deduce that chromophores tend to aggregate close to the binding site. Similar effects have been previously shown for other amyloid staining dyes, e.g., thioflavin T, which has a protonated nitrogen in the thiazole ring and can form aggregates when binding to insulin and other fibrils.²⁰

Thin-Film Characterization. Aggregation in rhodamine 6G has been extensively studied. It is well known that J- and H-aggregates can be easily formed and are responsible for spectral changes and shifts in absorbance and fluorescence. These effects are most pronounced in thin films where, due to evaporation, chromophores tend to self-assemble into higher order structures.²¹

Figure 2 represents a set of absorption spectra of pristine rhodamine 6G and rhodamine 6G in the presence of either lysozyme or insulin fibrils in the solid state. All three spectra are red-shifted by approximately 10–15 nm compared to the absorption in solution, confirming that rhodamine tends to aggregate upon solvent evaporation. According to the nonlinear least-squares fitting of absorption spectra done by Martinez-Martinez et al.,²² the main dye band around 540 nm can be attributed to J-type dimers, whereas a shoulder at 510 nm refers to H-type aggregation. The presence of amyloids determines the spatial distribution of chromophores and controls the aggregation formation at their surface. According to absorption spectra shown in Figure 2a in the case of lysozyme fibrils, the J-form dominates, whereas insulin fibrils induce H-type aggregation formation.²³

Laser scanning confocal microscopy was used to analyze the material properties of thin films. Surprisingly, the morphologies

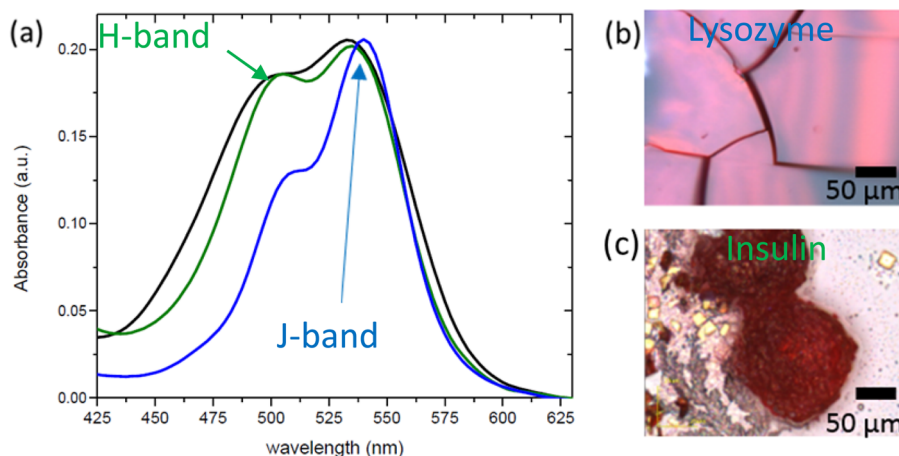


Figure 2. Absorbance of rhodamine 6G in a thin film (black) and in the presence of insulin fibrils (green) or lysozyme fibrils (blue) (a). Image of tile-like structure of lysozyme fibrils–Rh6G thin film (b). Image of grain-like particles of insulin fibril–Rh6G thin film (c).

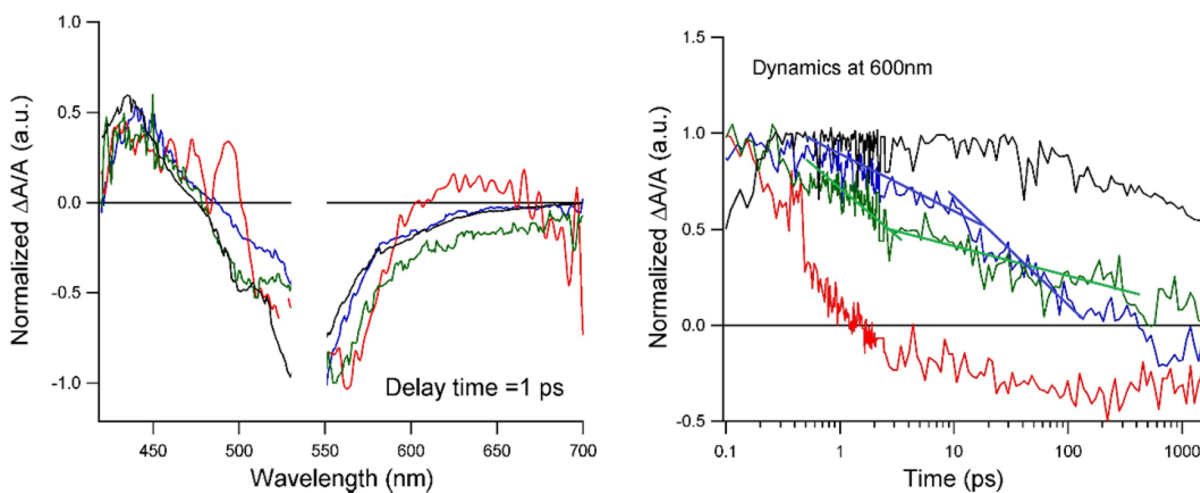


Figure 3. Transient absorption spectra (a) and dynamics at 600 nm (b) for rhodamine 6G in solution (black), the solid state (red), and thin films of lysozyme fibrils doped with Rh6G (blue) and insulin fibrils Rh6G complex (green).

of drop-cast layers of lysozyme and insulin fibrils doped with rhodamine 6G are completely different (Figure 2b and c). In the case of lysozyme fibrils, tile-like structures are formed predominantly at the sample edges, whereas grain-like particles were obtained for insulin fibrils over the entire film area (Figure S1). The edge of the lysozyme film is usually composed of a few tiles crossing each other with irregular dimensions ranging from 60 to 80 μm in width and up to 13 μm in height for a single tile. The width of the grain-like particles in the insulin film is between 60 and 130 μm each with a height in the range 70–120 μm . Confocal images indicate formation of different higher order structures that depend on the self-assembling pathway that is induced by solvent evaporation. Small molecules such as rhodamine 6G attached to the fibril surface follow this assembling scheme and exhibit new photophysical features.

Transient Absorption of Dye Aggregates. It is generally known that dye aggregation leads to self-quenching and shortening of the lifetimes.²⁴ For such samples transient absorption (TA) spectroscopy is most convenient since it enables the study of nonradiative processes through stimulated emission in aggregated systems. Thus, the excited-state dynamics of rhodamine 6G aggregates and the influence of nanotemplating at amyloid fibrils were investigated. TA of rhodamine 6G was performed in either solution or thin film using a pump pulse at 530 nm that was followed by a probe in the range 400–700 nm. Relatively large spectral noise is due to the low concentration of dye molecules (see the Experimental Section). In general for all studied samples TA spectra show two bands: a positive one below 470 nm that can be assigned to the excited-state absorption and a negative one above 470 nm that is due to the bleaching of the chromophore ground state combined with the stimulated emission (Figure 3a).

Solution studies show no difference in dynamics and nonradiative decays when comparing pristine rhodamine 6G and that complexed with amyloid fibrils (Figure S2). The lifetimes that are in nanosecond time scale indicate that excited-state dynamics is mostly attributed to monomers. These results fit well with the steady-state absorption (Figure 1 (dotted lines)) where no photophysical changes were observed since only a small fraction of dye molecules can bind to amyloid fibrils. Thus, their signal in solution samples is within the background scattering.

The same set of experiments performed on solid thin films showed large variation in excited-state dynamics of rhodamine that depends on aggregation rate. Figure 3 represents a comparison of TA spectra and dynamics at 600 nm between monomer dye in solution with thin films made of pristine rhodamine 6G and complexed with either lysozyme or insulin fibrils. Upon pumping the microcrystals, the nonradiative decay is within 2 ps, i.e., 3 orders of magnitude faster than for monomers (>1 ns) in solution. Similar results were reported for dimers and higher order aggregates.^{25,26} Interaction with amyloids prevents crystal formation, and due to larger attractive forces upon solvent evaporation, fibrils can mediate rhodamine aggregation formation at the nanotemplate surface. TA dynamics at 600 nm indicates that nonradiative decay of the Rh6G to the ground state in the presence of fibrils lasts ca. 300–400 ps, whereas the exact pathway depends on the intrinsic structure of the amyloid source and can be described by a two-step model (Figure 3b). A fast process within the first few picoseconds (1–3 ps) is followed by the decay that occurs in rhodamine 6G-doped insulin fibrils. In the lysozyme–dye complex the signal is constant over 20 ps and the decay starts after that time.

Stimulated Emission in Solutions. Similar to absorption studies in solution, the spontaneous emission of rhodamine 6G complexed with insulin or lysozyme fibrils is dominated by the monomer molecules since there are no spectral changes and only a few nanometer red-shift, indicating the presence of dimers and higher order aggregates but with negligible impact on the photophysics of the supramolecular complexes (Figure S3). However, in stimulated emission, aggregates of certain sizes can be visualized because the emission is not forbidden by the selection rules. An acidic environment (pH = 2.0) protonates negatively charged amino acid groups (aspartic acid and glutamic acid) and together with repulsive interaction with positively charged ones (lysine, histidine, and arginine) can be a driving force for aggregation in molecular crowding conditions. Luminescence of J- and imperfect H-aggregates is usually red-shifted compared to monomers.

Since the transition dipole moment in dimer or higher order aggregates is tilted with respect to the monomer,²⁷ the decay time is longer, giving a possibility to create excited states of sufficient lifetime for laser emission. If gain provided by the aggregates is sufficient, the stimulated emission occurs at lower

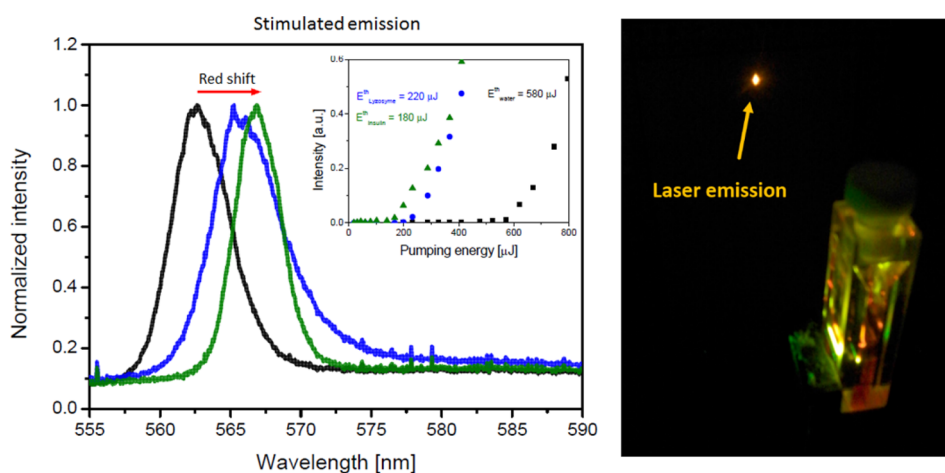


Figure 4. Lasing spectra obtained by averaging 50 pulse shots in solution for pristine rhodamine 6G (black) and in the presence of lysozyme (blue) or insulin (green) amyloid fibrils. The inset represents a comparison of lasing thresholds for pristine rhodamine 6G and in the presence of two types of amyloid fibrils (a). Lasing effect in a cuvette containing rhodamine 6G in water solution (pH = 2).

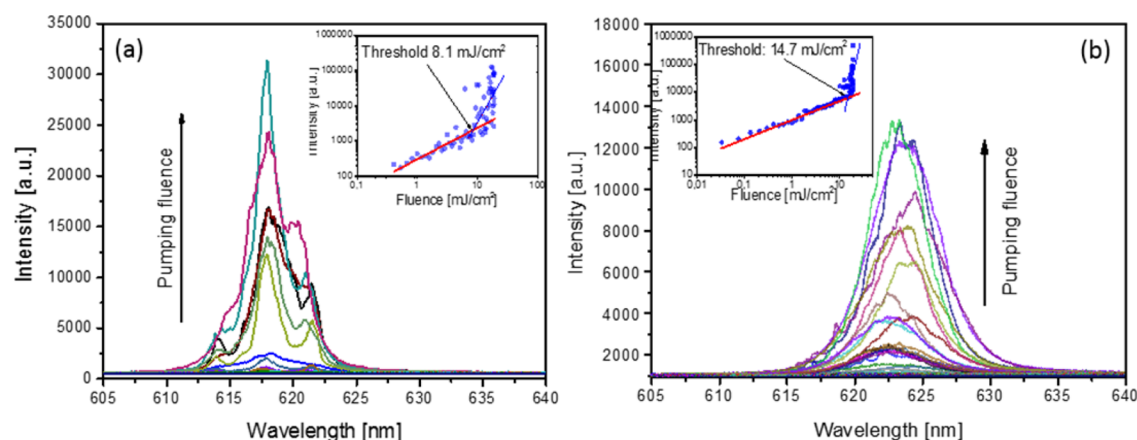


Figure 5. Random lasing spectra obtained for rhodamine 6G-stained amyloid layers. Lysozyme (a) and insulin (b). Insets show emission intensity dependence on pumping fluence.

thresholds and it is red-shifted with respect to the monomers; see Figure 4. Such molecular disorder might be useful to obtain materials with low threshold and broad wavelength tunability.²⁸

The red shift observed in Figure 4a is determined by the red shift of the gain profile that is observed in the presence of the amyloid fibrils (for a lysozyme shift from 563 to 567 nm and for insulin up to 568 nm), while the feedback for stimulated emission was provided by the interference of light reflected from the walls of a quartz cuvette (for more details see Supporting Information Figure S5). The same experiments where light reflectance was identical were performed in amyloid–dye solutions. A threshold of a pristine dye in water solution (580 μ J) is reduced by nearly a factor of 3 to 180 μ J and 220 μ J in samples containing rhodamine complexed with insulin and lysozyme fibrils, respectively.

Stimulated Emission in Thin Films. The aggregation rate is accelerated in solid-state films due to solvent evaporation that enhances the attractive forces between amyloid fibrils and chromophores. Studying stimulated emission and lasing is particularly convincing in amyloid thin layers because pristine dye molecules form microcrystals. In thin films with only crystals, photons pass through the sample and no light amplification can be observed.

Only rhodamine 6G aggregates deposited on amyloids can induce light amplification at a variety of wavelengths (Figures S6 and S7). The exact lasing wavelength is related to the aggregation rate, size, shape, and geometry of chromophores attached to the biotemplate and can be useful in broadband laser applications.²⁷

For stimulated emission studied in thin films, measurements used an exciting beam of stripe shape geometry (0.3×0.05 cm²) of wavelength 532 nm and pulse width 6 ns. Emission amplification is observed with increasing pump energy where the threshold for the process was estimated to be at 8.1 mJ/cm² for lysozyme and 14.7 mJ/cm² for insulin fibril films (see inset in Figure 5a and b, respectively). In the case of the lysozyme matrix, the stimulated emission occurs at 618 nm and is red-shifted by about 50 nm compared to the monomer's emission. This indicates that the light amplification is obtained directly from aggregates. Moreover the spectra recorded at different pump energies show irregular shapes that vary from pulse to pulse of excitation, indicating that stimulated emission involves random lasing. The evolution of the emission spectra as a function of increasing excitation fluence is shown in the insets of Figure 5.

Similar experiments were conducted for dye-doped insulin fibril layers. In this case stimulated emission spectra was shifted

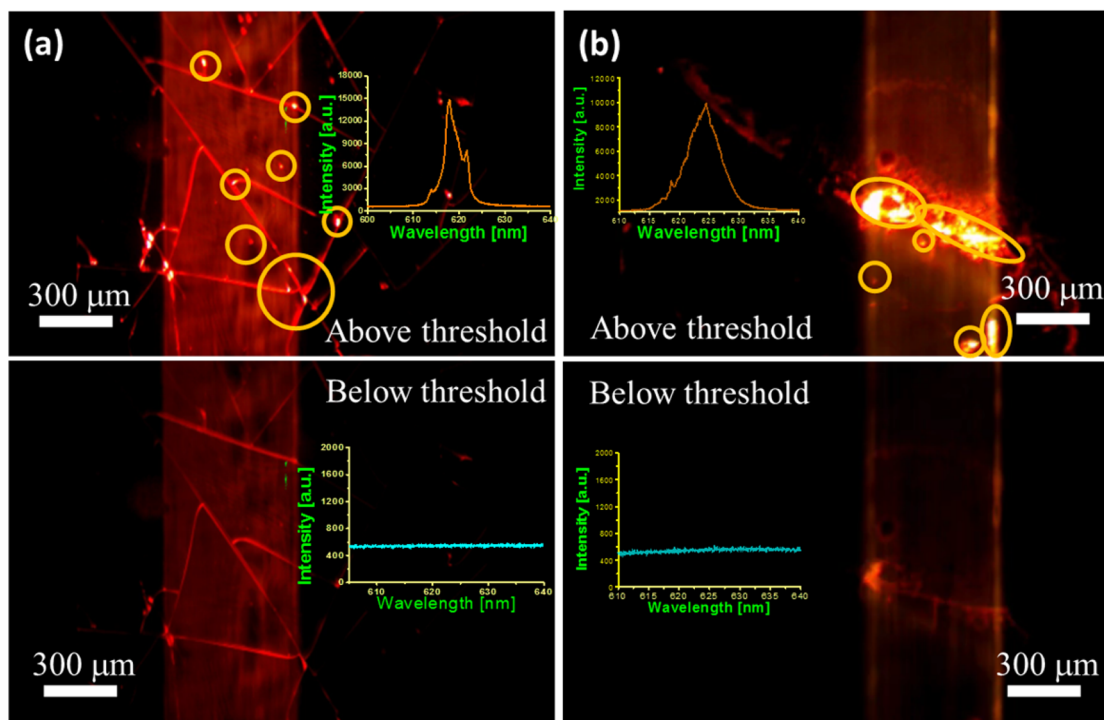


Figure 6. Images of excited area of lysozyme type of layer (a) and insulin type of layer (b), above and below a random lasing threshold.

to longer wavelengths centered at 622 nm near the threshold and further shifted to around 625 nm when measured above the threshold. The emission spectral shape also varied from pulse to pulse of excitation, indicating that random feedback constituted random laser emission. In both cases, a random lasing phenomenon is related to the morphology of the biopolymeric films. The images of the emission (above and below the threshold) are shown in Figure 6a and b for lysozyme and insulin fibril films, respectively.

The image in Figure 6a is a thin film of lysozyme fibrils doped with rhodamine 6G and strongly defected by the numerous cracks, which are especially visible above the threshold, when the enhanced light can be easily scattered from the propagation plane. Above the threshold it is also possible to distinguish spots of higher intensity (indicated by yellow circles) that are mostly present inside the cracks as well as the tiles. The width of the single tile is around several tens of micrometers (Figures 2b and S1(a)), creating a network of microcavities where light is propagating within the aggregates of rhodamine 6G attached to the amyloids. These structures are responsible for light localization leading to a random laser emission. Most probably both scattering from the crack edges and from aggregates can contribute to the random feedback (intensity and amplitude) for random laser emission. For films containing dye-doped insulin fibrils the light amplification is related only to the rate of aggregation within the grain structures. The mechanism of light amplification can be explained in terms of the granular morphology (Figures 2c and S1(b)) that leads to disorder, which plays a crucial role in the constitution of the random feedback. The difference in mechanism behind stimulated emission in lysozyme and insulin fibrils is striking when looking at the pictures taken above the threshold (Figure 6). The spikes appearing in both lysozyme and insulin types of layers show that weak localization of light takes place in both systems. This localization may be assigned to “short-range” disorder arising within aggregates and clusters

of rhodamine 6G. However, closer inspection of stimulated emission spectra leads to the conclusion that spikes are in fact less pronounced than in laser emission reported for example for ZnO nanopowders²⁹ or π -conjugated systems.^{30,31} This means that in the case of amyloid–dye complexes there are more components that are influencing the feedback for laser emission.³² At least in the case of lysozyme-type layers doped with Stilbene 420 laser dye can produce stimulated emission as random lasing coming from the cracks. As long as Stilbene 420 laser dye is negatively charged, it can easily bind to positively charged amino acids present in the amyloid structure at pH = 2.0. This means that dye molecules are equally distributed over the binding sites and no aggregation occurs. Thus, the multiple scattering may occur mostly on crack edges, and no classical lasing was observed in the aforementioned experiment.

In order to check if the size of the pumping region can influence the threshold of the lasing emission, additional experiments with circular-shape excitation area of 0.2 cm² (5 mm in diameter) were performed. These experiments provide the information on whether the feedback strength is dependent on the size of the excitation area. Results indicate that the thresholds indeed depend on the size of the excitation spot and were further decreased to 0.35 and 0.77 mJ/cm² for doped lysozyme and insulin layers, respectively, when compared to thresholds estimated for a stripe excitation area (0.015 cm²). Moreover, in the case of insulin fibril thin films a red shift was observed when increasing the pump fluence. This indicates that population inversion occurs within a large set of different aggregates, and in the stimulated emission process some can be exclusively excited, whereas others remain inactive. Amyloid-controlled aggregation distribution is another feature that can

be promising in the context of using biderived nanotemplates for laser technology applications (Figures S6 and S7).

CONCLUSIONS

Rhodamine 6G tends to aggregate in the presence of amyloid fibrils due to the limited binding sites. That affects the chromophore photophysics and the thin film morphology of dye-doped amyloid layers. The consequence of aggregation is a different mechanism of light amplification in lysozyme and insulin fibrils both in solution and in the solid state. The amyloid fibril intrinsic structure mediates the size, geometry, and formation of rhodamine 6G aggregates that lead to broadband random lasing and threshold reduction. These biderived nanotemplates are promising materials for photonic application since they are easy to fabricate, handle, and control in the preparation of supramolecular complexes. Recent studies on biomolecules such as DNA, silk, and amyloids indicate the richness of interactions that can be utilized to tailor photonic features of a source of renewable and bio- and eco-friendly biophotonic materials.

ASSOCIATED CONTENT

Supporting Information

The Supporting Information is available free of charge on the ACS Publications website at DOI: 10.1021/acsphotonics.5b00458.

3D optical images of thin films, transient absorption spectra measured on solutions with either free rhodamine 6G or that complexed with amyloid fibrils, fluorescence spectra, setup for lasing together with reference experiments performed on free rhodamine in solution, and lasing of thin films measured at a striped excitation area (0.015 cm²) (PDF)

AUTHOR INFORMATION

Corresponding Author

*E-mail (A. J. Heeger): ajhe1@physics.ucsb.edu.

Notes

The authors declare no competing financial interest.

ACKNOWLEDGMENTS

We thank Adrian Justyniarski and Byoung-Hoon Lee for technical help. We acknowledge funding from the Swedish Research Council (VR) and Polish National Science Centre (Grant No. DEC-2013/09/D/ST4/03780). Work at UCSB was supported by the Department of the Navy, Office of Naval Research Award No. N00014-14-1-0580.

REFERENCES

- (1) Breydo, L.; Uversky, V. N. Structural, morphological, and functional diversity of amyloid oligomers. *FEBS Lett.* **2015**, *589*, 2640–2648.
- (2) Tran, L.; Ha-Duong, T. Exploring the Alzheimer amyloid- β peptide conformational ensemble: A review of molecular dynamics approaches. *Peptides* **2015**, *69*, 86–91.
- (3) Härd, T. Amyloid fibrils: Formation, polymorphism, and inhibition. *J. Phys. Chem. Lett.* **2014**, *5*, 607–614.
- (4) Tycko, R. Amyloid Polymorphism: Structural Basis and Neurobiological Relevance. *Neuron* **2015**, *86*, 632–645.
- (5) Knowles, T. P.; Fitzpatrick, A. W.; Meehan, S.; Mott, H. R.; Vendruscolo, M.; Dobson, C. M.; Welland, M. E. Role of intermolecular forces in defining material properties of protein nanofibrils. *Science* **2007**, *318*, 1900–1903.

- (6) Sachse, C.; Grigorieff, N.; Fändrich, M. Nanoscale Flexibility Parameters of Alzheimer Amyloid Fibrils Determined by Electron Cryo-Microscopy. *Angew. Chem., Int. Ed.* **2010**, *49*, 1321–1323.
- (7) Sznitko, L.; Hanczyc, P.; Mysliwiec, J.; Samoc, M. Low-threshold stimulated emission from lysozyme amyloid fibrils doped with a blue laser dye. *Appl. Phys. Lett.* **2015**, *106*, 023702.
- (8) Staderini, M.; Martín, M. A.; Bolognesi, M. L.; Menéndez, J. C. Imaging of β -amyloid plaques by near infrared fluorescent tracers: a new frontier for chemical neuroscience. *Chem. Soc. Rev.* **2015**, *44*, 1807–1819.
- (9) Bäcklund, F. G.; Solin, N. Development and Application of Methodology for Rapid Screening of Potential Amyloid Probes. *ACS Comb. Sci.* **2014**, *16*, 721–729.
- (10) Hanczyc, P. Binuclear ruthenium (II) complexes for amyloid fibrils recognition. *Chem. Phys.* **2014**, *445*, 1–4.
- (11) Harada, R.; Okamura, N.; Furumoto, S.; Yoshikawa, T.; Arai, H.; Yanai, K.; Kudo, Y. Use of a benzimidazole derivative BF-188 in fluorescence multispectral imaging for selective visualization of tau protein fibrils in the Alzheimer's disease brain. *Molecular Imaging and Biology* **2014**, *16*, 19–27.
- (12) Kuhnke, D.; Jedlitschky, G.; Grube, M.; Krohn, M.; Jucker, M.; Mosyagin, I.; Cascorbi, I.; Walker, L. C.; Kroemer, H. K.; Warzok, R. W. MDR1-P-Glycoprotein (ABCB1) Mediates Transport of Alzheimer's Amyloid- β Peptides—Implications for the Mechanisms of A β Clearance at the Blood–Brain Barrier. *Brain Pathol.* **2007**, *17*, 347–353.
- (13) Cao, H.; Xu, J.; Chang, S.-H.; Ho, S. Transition from amplified spontaneous emission to laser action in strongly scattering media. *Phys. Rev. E: Stat. Phys., Plasmas, Fluids, Relat. Interdiscip. Top.* **2000**, *61*, 1985.
- (14) Kawabe, Y.; Wang, L.; Horinouchi, S.; Ogata, N. Amplified Spontaneous Emission from Fluorescent-Dye-Doped DNA–Surfactant Complex Films. *Adv. Mater.* **2000**, *12*, 1281–1283.
- (15) Yu, Z.; Li, W.; Hagen, J.; Zhou, Y.; Klotzkin, D.; Grote, J.; Steckl, A. Photoluminescence and lasing from deoxyribonucleic acid (DNA) thin films doped with sulforhodamine. *Appl. Opt.* **2007**, *46*, 1507–1513.
- (16) Camposeo, A.; Del Carro, P.; Persano, L.; Cyprych, K.; Szukalski, A.; Sznitko, L.; Mysliwiec, J.; Pisignano, D. Physically Transient Photonics: Random versus Distributed Feedback Lasing Based on Nanoimprinted DNA. *ACS Nano* **2014**, *8*, 10893–10898.
- (17) Toffanin, S.; Kim, S.; Cavallini, S.; Natali, M.; Benfenati, V.; Amsden, J. J.; Kaplan, D. L.; Zamboni, R.; Muccini, M.; Omenetto, F. G. Low-threshold blue lasing from silk fibroin thin films. *Appl. Phys. Lett.* **2012**, *101*, 091110.
- (18) Sagnella, A.; Chieco, C.; Di Virgilio, N.; Toffanin, S.; Posati, T.; Pistone, A.; Bonetti, S.; Muccini, M.; Ruani, G.; Benfenati, V. Bioprocessing of regenerated silk fibroin solution and films: a green route for biomanufacturing. *RSC Adv.* **2014**, *4*, 33687–33694.
- (19) Kaake, L. G.; Zhong, C.; Love, J. A.; Nagao, I.; Bazan, G. C.; Nguyen, T.-Q.; Huang, F.; Cao, Y.; Moses, D.; Heeger, A. J. Ultrafast Charge Generation in an Organic Bilayer Film. *J. Phys. Chem. Lett.* **2014**, *5*, 2000–2006.
- (20) Sabate, R.; Rodriguez-Santiago, L.; Sodupe, M.; Saupe, S. J.; Ventura, S. Thioflavin-T excimer formation upon interaction with amyloid fibers. *Chem. Commun.* **2013**, *49*, 5745–5747.
- (21) Hu, R.; Leung, N. L.; Tang, B. Z. AIE macromolecules: syntheses, structures and functionalities. *Chem. Soc. Rev.* **2014**, *43*, 4494–4562.
- (22) Martínez Martínez, V.; López Arbeloa, F.; Bañuelos Prieto, J.; Arbeloa López, T.; López Arbeloa, I. Characterization of rhodamine 6G aggregates intercalated in solid thin films of laponite clay. 1. Absorption spectroscopy. *J. Phys. Chem. B* **2004**, *108*, 20030–20037.
- (23) Arbeloa, F. L.; Martínez Martínez, V.; Arbeloa, T.; Arbeloa, I. L. Photoresponse and anisotropy of rhodamine dye intercalated in ordered clay layered films. *J. Photochem. Photobiol., C* **2007**, *8*, 85–108.
- (24) Castro, B. M.; De Almeida, R. F.; Fedorov, A.; Prieto, M. The photophysics of a Rhodamine head labeled phospholipid in the

identification and characterization of membrane lipid phases. *Chem. Phys. Lipids* **2012**, *165*, 311–319.

(25) Penzkofer, A.; Leupacher, W. Fluorescence behaviour of highly concentrated rhodamine 6G solutions. *J. Lumin.* **1987**, *37*, 61–72.

(26) Fedoseeva, M.; Letrun, R.; Vauthey, E. Excited-State Dynamics of Rhodamine 6G in Aqueous Solution and at the Dodecane/Water Interface. *J. Phys. Chem. B* **2014**, *118*, 5184–5193.

(27) Martínez Martínez, V.; López Arbeloa, F.; Bañuelos Prieto, J.; López Arbeloa, I. Characterization of Rhodamine 6G aggregates intercalated in solid thin films of laponite clay. 2 fluorescence spectroscopy. *J. Phys. Chem. B* **2005**, *109*, 7443–7450.

(28) Cyprych, K.; Kopczynska, Z.; Kajzar, F.; Rau, I.; Mysliwiec, J. Tunable wavelength light emission and amplification in Rhodamine 6G aggregates. *Advanced Device Materials* **2015**, *1*, 69–73.

(29) Cao, H.; Zhao, Y. G.; Ho, S. T.; Seelig, E. W.; Wang, Q. H.; Chang, R. P. H. Random laser action in semiconductor powder. *Phys. Rev. Lett.* **1999**, *82*, 2278–2281.

(30) Tulek, A.; Vardeny, Z. Studies of random laser action in π -conjugated polymers. *J. Opt.* **2010**, *12*, 024008.

(31) Hide, F.; Schwartz, B. J.; Díaz-García, M. A.; Heeger, A. J. Laser emission from solutions and films containing semiconducting polymer and titanium dioxide nanocrystals. *Chem. Phys. Lett.* **1996**, *256*, 424–430.

(32) Cao, H. Lasing in random media. *Waves Random Media* **2003**, *13*, R1–R39.